

UC San Diego

UC San Diego Electronic Theses and Dissertations

Title

Study of Polyethylene Oxide(PEO) as an Ionic Conducting Binder for Li-ion Battery Cathode

Permalink

<https://escholarship.org/uc/item/4kj6h9dm>

Author

Fang, Jie

Publication Date

2018

Peer reviewed|Thesis/dissertation

UNIVERSITY OF CALIFORNIA SAN DIEGO

Study of Polyethylene Oxide (PEO) as an Ionic Conducting Binder
for Li-ion Battery Cathode

A Thesis submitted in partial satisfaction of the requirements
for the degree Master of Science

in

Chemical Engineering

by

Jie Fang

Committee in charge:

Professor Zheng Chen, Chair
Professor Ping Liu
Professor Tod Pascal

2018

Copyright

Jie Fang, 2018

All rights reserved.

The Thesis of Jie Fang is approved, and it is acceptable in quality and form for publication on microfilm and electronically:

Chair

University of California San Diego

2018

TABLE OF CONTENTS

Signature Page	iii
Table of Contents	iv
List of Figures	v
List of Tables.....	vii
Abstract of the Thesis.....	viii
Chapter 1 Introduction.....	1
1.1 Significance and Working Mechanism of Li-ion batteries.....	1
1.2 Polymer Binders for Li-ion battery	6
Chapter 2 Using PEO as a Binder and Electrolyte Reservoir for NMC Batteries.....	8
2.1 PEO Li ⁺ Conducting Mechanism	8
2.2 Gel Polymer Electrolyte	10
2.4 Experimental Procedure of PEO Compatibility Study with NMC Cycling Under 3-4.3V	13
2.5 Results and Discussion.....	14
Chapter 3 PEO Stability with Electrolyte under Battery Cycling	17
3.1 Experimental	17
3.2 Result and Discussion	18
Conclusion.....	24
References	25

LIST OF FIGURES

Figure 1. Energy density comparisons between different battery systems.....	2
Figure 2. Lithium-ion battery working mechanism.....	3
Figure 3. Layered-metal oxide crystal structure.....	3
Figure 5. Common Li-salt dissociation constant order.....	8
Figure 6. PEO Li ⁺ conducting mechanism	9
Figure 7. PEO/LiTFSI phase diagram.....	10
Figure 8. Schematic of thermogravimetric curve of gel polymer electrolyte.....	11
Figure 9. Combustion test Celgard 2730 and PVDF-GFM gel polymer electrolyte.....	11
Figure 10. (a) Cycling performance of PEO-NMC cell, 2.608 mg mass loading, 10 uL of LP 40 added, cycling under 3-4.3V for 100 cycles, 0.1C first cycle and 1C the rest of the cycles (b) 4th cycle charge-discharge curve of the cell in figure 12 (a)	14
Figure 11. (a) Cycling performance of PEO-NMC cell, 7.361 mg mass loading, 28 uL of LP 40 added, cycling under 3-4.3V for 100 cycles, 0.1C first cycle and 0.2C the rest of the cycles (b) 4th cycle charge-discharge curve of the cell in figure 13 (a)	14
Figure 12. (a) Cyclic voltammogram of PVDF with 30 uL LP 40 under scan rate of 0.5 mV (b) Zoomed in on figure 14 (a).....	18
Figure 13. (a) Cyclic voltammogram of PVDF with 30 uL electrolyte under scan rate of 5 mV/s, 2 mV/s, 1 mV/s and 0.5 mV/s (b) Plot of specific peak current of different scan rates vs. square root of scan rate	18
Figure 14. (a) Pristine PVDF XPS spectra (b) PVDF after cycling XPS spectra.....	19
Figure 15. (a) Pristine PVDF C 1s XPS spectra (b) PVDF after cycled with 30 uL LP 40 C 1s XPS spectra (c) PVDF after cycled with 30 uL LP 40 O 1s XPS spectra.....	20
Figure 16. (a) Cyclic voltammogram of PEO with 30 uL LP 40 under scan rate of 0.5 mV (b) Zoomed in on figure 18 (a).....	21

Figure 17. (a) Cyclic voltammogram of PEO with 30 uL electrolyte under scan rate of 5 mV/s, 2 mV/s, 1 mV/s and 0.5 mV/s (b) Plot of specific peak current of different scan rates vs. square root of scan rate 21

Figure 18. (a) Pristine PEO C 1s XPS spectra (b) PEO after cycled with 30 uL LP 40 C 1s XPS spectra..... 22

Figure 19. (a) Pristine PEO O 1s XPS spectra (b) PEO after cycled with 30 uL LP 40 O 1s XPS spectra..... 22

Figure 20. (a) PEO and PVDF with 30 uL LP 40, 10 cycles of CV scan average peak current vs. scan rate (b) PVDF and PEO with 30 uL LP 40 after 10 cycles of CV scan held at 4.3 V for 10 hours chronoamperogram..... 23

Figure 21. PEO 4.3 and 4.4V chronoamperogram 23

LIST OF TABLES

Table 1. Common Liquid Electrolyte Solvent.....	5
Table 2. Typical binders, their molecular structures and the corresponding electrode materials....	7
Table 3. Examples of different active mass and electrolyte amount and corresponding cycling performance.....	15

ABSTRACT OF THE THESIS

Study of Polyethylene Oxide (PEO) as an Ionic Conducting Binder
for Li-ion Battery Cathode

by

Jie Fang

Masters of Science

University of California San Diego, 2018

Professor Zheng Chen, Chair

Li-ion battery has dominated the portable electronic market due to its high energy density. Li-ion battery is a complex system where each of its components should be compatible with each other. Polymer binder, although as an inactive component in a cell, plays an important role for battery performance. Polyethylene oxide (PEO) as an ionic conductive polymer has demonstrated its use in gel polymer batteries and solid state batteries. However, there are concerns about its compatibility with layered oxide material as well as stability under high voltage. This thesis studied the compatibility of PEO as a binder for $\text{LiNi}_{1/3}\text{Mn}_{1/3}\text{Co}_{1/3}\text{O}_2$ cathode and the stability of PEO up to 4.4V.

Chapter 1 Introduction

1.1 Significance and Working Mechanism of Li-ion batteries

Rechargeable Li-ion battery has dominated portable electronic market. First invented by Prof. Goodenough in 1980 and commercialized by SONY in 1991, it is widely found in cell phones, laptops, watches etc. As shown in figure 1, it has much higher energy density than the traditional lead acid batteries, Ni-Cd and Ni-metal hydride batteries. Noted that even if the Li metal batteries have higher energy density than Li-ion batteries, they are considered 'unsafe' because of the difficulty in preventing Li dendrite growth, which eventually short-circuits the battery.

Li-ion battery is also believed to be the solution to reducing greenhouse gas emission by taking the place of gasoline as the energy source for vehicles. It is estimated that an average gasoline vehicle emits about 6 tons of CO₂ each year^[1]. If the energy source of battery electric vehicles(BEV) production is from a sustainable clean source, such as solar, wind power, BEV production leaves no carbon footprints^[2]. In able to replace gasoline to power a vehicle, the energy density of Li-ion battery should be comparable to gasoline. It is worth noted that fuel cell vehicles also has great potential as replacement of gasoline cars due to its even higher energy density. However, hydrogen production for fuel cell as well as hydrogen storage remain a challenge for its large-scale commercialization^[3]. Li-ion battery on the other hand, has less of a storage issue and it is environmentally friendly with high power density, compared to other battery technologies such as lead and nickel systems, and therefore has the potential revolutionizing the ground transportation.

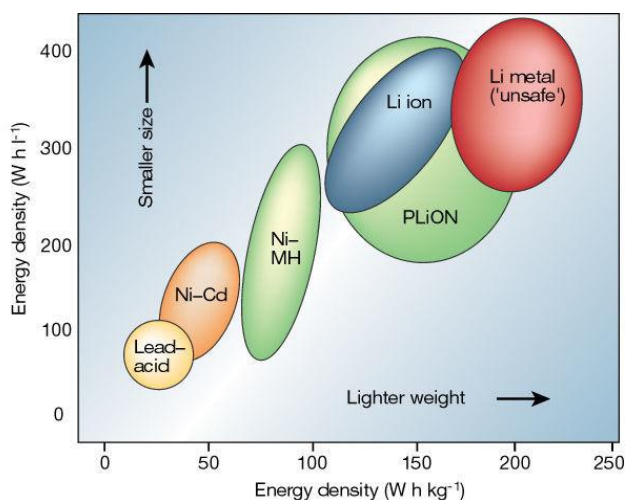
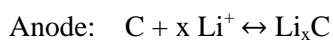
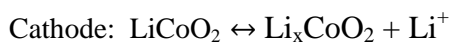


Figure 1. Energy density comparisons between different battery systems ^[2]

A typical lithium-ion battery, as shown in figure 2, consists of a cathode, anode, separator that prevents direct contact between the cathode and anode, and liquid electrolyte. The anode is usually graphite and the cathode is a layered-oxide material. As in figure 2, the active cathode material is LiCoO_2 (LCO). Despite the challenges of this material, under regulated voltage and appropriate cell engineering, LCO has been commercialized and widely found in portable electronics such as cell phones, laptops etc. Its crystal structure is shown in figure 3 and figure 4. Oxygen anions form a closely packed face centered cubic (FCC) lattice with cations, in this case Li^+ , which located in the octahedral sites. The metal oxide slabs and Li^+ are ABCABC stacking, which Li^+ and the metal oxide stack alternatively to each other. The electrochemical reaction during charging and discharging is:



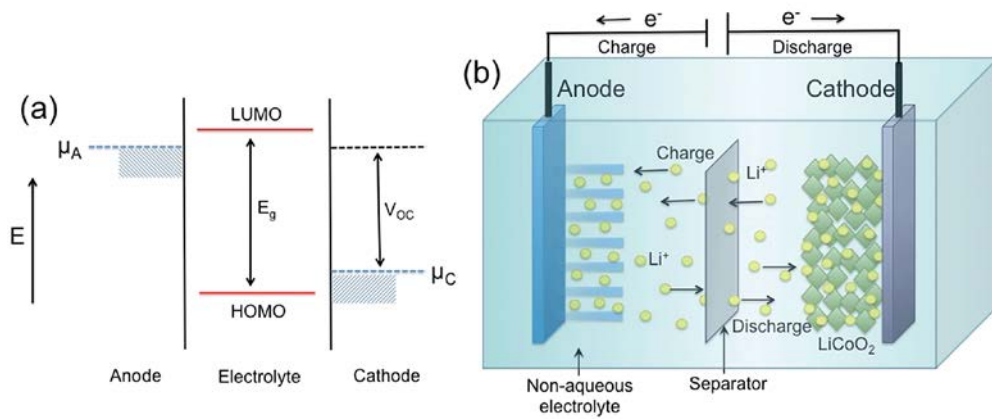


Figure 2. Lithium-ion battery working mechanism^[4]

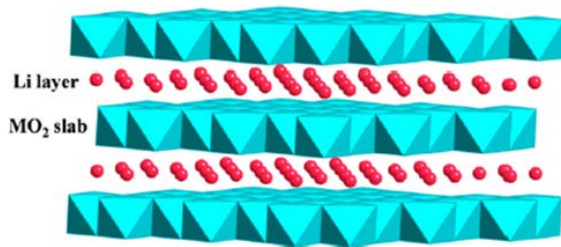


Figure 3. Layered-metal oxide crystal structure^[5]

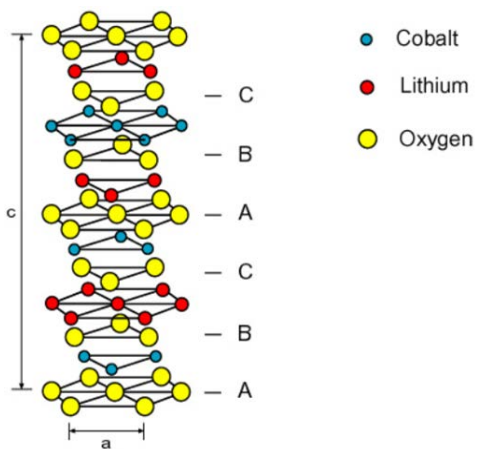


Figure 4. $LiCoO_2$ crystal structure^[5, 6]

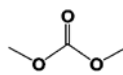
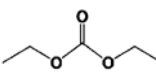
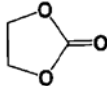
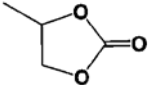
During charging Li^+ moves from the cathode to anode. Anode is usually made of graphite, which is also a layered structure with the Li^+ insertion capability without much structural change.

The theoretical capacity of LCO is 274 mAh/g. However, its practical capacity is around 150 mAh/g under cycling voltage of 3-4.3V because only less than 50% of the Li^+ can be reversibly extracted from the crystal structure^[6] because of the overlapping of oxygen 2p band with the $\text{Co}^{3+/4+}$, which when the voltage goes beyond typically 4.5V during charging, not only the electron would be extracted from cobalt, but also from oxygen which results in the gassing of O_2 ^[5]. Another major drawback for LCO is that cobalt is expensive. From a statistics of a 5-year price range, Co costs from \$10-25 per pound. Comparatively, Ni costs from \$5-15 per pound and Mn costs only \$1-2 per pound^[7]. To solve the problem of the high cost of cobalt, partially replacing Co with Ni and Mn, Tsutomu Ohzuku and Yoshinari Makimura^[8] synthesized a structurally stable, cheaper yet retains the same specific capacity material $\text{LiNi}_{1/3}\text{Mn}_{1/3}\text{Co}_{1/3}\text{O}_2$ (NMC111). The transition metal oxidation sequence of Ni^{2+} during charging is from Ni^{2+} to Ni^{3+} and then from Ni^{3+} to Ni^{4+} , while the oxidation state of Mn^{4+} remains unchanged. It should be noted that there are different types of NMC sharing a chemical formula of $\text{LiMn}_x\text{Ni}_y\text{Co}_z\text{O}_2$, such as $\text{LiNi}_{0.8}\text{Mn}_{0.1}\text{Co}_{0.1}\text{O}_2$ which its high Ni component is capable of delivering high capacity while the issue of Ni^{2+} taking place of Li^+ causing irreversible structural change remains a challenge^[9]. This thesis focuses on utilization of NMC 111.

Electrolyte for Li-ion battery consists of a suitable lithium salt, usually LiPF_6 , dissolved in appropriate solvents. Electrolyte for Li-ion battery must have high Li^+ conductivity which is at least in the range of 10^{-3} to 10^{-2} S/cm under room temperature, high dielectric constant, low viscosity and appropriate electrochemical stability window^[10]. Li^+ are transported through electrolyte, electrolyte with low Li^+ conductivity results in high internal impedance and inability to utilize the electrode material capacity to the fullest. Solvents with high dielectric constant have high ability to dissolve Li salts while low viscosity facilitates the Li^+ ion transport. The potential of anode must be below the lowest unoccupied molecular orbital (LUMO) of electrolyte and the

potential of cathode must be above the highest occupied molecular orbital (HOMO) of electrolyte. Otherwise, the electrolyte will be reduced on anode and oxidized on cathode^[11]. The melting point should be low and boiling point should be high so that it stays as liquid form in a wide range of temperature. Solution of 1M of LiPF₆ in EC/DEC, with which volume ratio is 1:1 meets the above requirements and are widely used in commercialized and laboratory-scale Li-ion batteries. Also called LP 40, this is the liquid electrolyte of interest in this thesis. Table 1 lists examples of common electrolyte: DMC, DEC, EC and PC used in Li-ion batteries^[12].

Table 1. Common Liquid Electrolyte Solvent^[12]

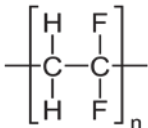
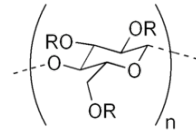
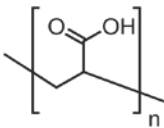
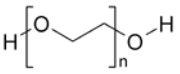
Solvent	Chemical Structure	Dielectric Constant	Room Temp Viscosity (mPa • S)	Flashing Point (°C)	Melting Point (°C)	Boiling Point (°C)
Dimethyl Carbonate (DMC)		3.107	0.59	18	4.6	91
Diethyl Carbonate (DEC)		2.805	0.75	31	-74.3	126
Ethylene Carbonate (EC)		89.78	1.90 (40 °C)	160	36.4	248
Propylene Carbonate (PC)		64.92	2.53	132	-48.8	242

1.2 Polymer Binders for Li-ion Battery

Polymer binders are the glue that puts active material and conductive agents such as carbon together with the current collector in the electrodes. Although it is an inactive component in a cell, it could affect the battery performance in terms of capacity decay and cycle life significantly^[13] ^[14] ^[15]. General features for the polymer binders should be excellent adhesion strength so that it glues the active materials with the current collector well even after wetting of electrolyte and cycling. Otherwise, it will cause detachment of active materials to current collector and results in mass transfer resistance increase and eventually causing capacity decay. Secondly it is required to be highly processable with solvents. The conventional way of making electrode slurry is mixing active material with additives such as carbon black, with the polymer binder in a solvent that can dissolve the polymer and disperse the active material and carbon at the same time. Therefore, processability with solvents is another important criterion for polymer binders. Thirdly, the binder should be compatible with electrochemical reactions under high voltage.

The mostly used and commercialized binder is polyvinylidene fluoride (PVDF) or its co-polymer polyvinylidene fluoride -co-hexafluoropropylene (PVDF-HFP), owing to the good adhesion strength, electrochemical stability and relatively low cost. However, its processing solvent N-Methyl-2-pyrrolidone (NMP) is toxic. Also, other conductive polymers such as polyethylene oxide (PEO) are Li⁺ conductive which provide better Li⁺ pathway than PVDF. And the processing solvent for other binders such as PEO and Carboxymethyl cellulose (CMC) only requires de-ionized water, which is non-toxic and cheaper than NMP. Table 2 lists common binders for Li batteries.

Table 2. Typical binders, their molecular structures and the corresponding electrode materials

Name	Molecular Structure	Electrode Materials
Polyvinylidene fluoride (PVDF)	 $\left[\begin{array}{c} \text{H} \quad \text{F} \\ \quad \\ -\text{C} - \text{C}- \\ \quad \\ \text{H} \quad \text{F} \end{array} \right]_n$	$\text{LiNi}_x\text{Mn}_y\text{Co}_{1-x-y}\text{O}_2$ ^[8] , LiCoO_2 ^[16] , $\text{LiTi}_4\text{O}_{12}$ ^[17] , Graphite
Carboxymethyl cellulose (CMC)	 $\left(\begin{array}{c} \text{RO} \quad \text{OR} \\ \diagup \quad \diagdown \\ \text{O} \quad \text{O} \\ \diagdown \quad \diagup \\ \text{OR} \end{array} \right)_n$ <p>R = H or CH₂CO₂H</p>	Graphite ^[18] , $\text{LiTi}_4\text{O}_{12}$ ^[19] , Si ^[20]
Polyacrylic acid (PAA)	 $\left[\begin{array}{c} \text{O} \quad \text{OH} \\ \quad \\ -\text{C} - \text{C}- \\ \quad \end{array} \right]_n$	Si ^[21]
Polyethylene Oxide (PEO)	 $\text{H} \left[\text{O} - \text{CH}_2 - \text{CH}_2 - \text{O} \right]_n \text{H}$	LiFePO_4 ^[22] , Li-S batteries ^[23]

Chapter 2 Using PEO as a Binder and Electrolyte Reservoir for NMC Batteries

This section will first introduce the PEO Li^+ conducting mechanism, and what other researchers has utilize Li^+ conducting polymers as gel electrolyte to make a safer battery. Despite all the advantages PEO could bring to a battery system, it has not been commercialized with layered oxide material because of concerns of high voltage stability. Then we further explained the reason why we choice $\text{PEO}_{10}\text{LiTFSI}$ as the target of study, and finally experimentally verified PEO as a binder and liquid electrolyte reservoir and its compatibility with NMC111 under 3-4.3V.

2.1 PEO Li^+ Conducting Mechanism

To conduct Li^+ , PEO should first have the ability to solvate the salt or cations. The solvation of cations in salt with a polymer comes from its interaction with the lone electron pairs in the heteroatom in a polymer chain^[24]. Ether has heteroatom containing lone pair electron, other common polymers that share this feature are: sulfide, amine, phosphine, carbonyl, and cyano^[25]. To form a complex with these polymer, only Li salt with low lattice energy are capable^[25]. They usually have bulk anions, where its charge delocalization degree is high. Below is a sequence of dissociation constant for anions that meet the above requirement and are commonly used in salt-in polymer electrolyte system^[24]:



Figure 5. Common Li-salt dissociation constant order^[24]

Ionic conductivity in a polymer chain mainly comes from segmental motion, which occurs above the glass transition temperature (T_g). Above T_g , solvation-desolvation process is enabled along the polymer chains. PEO at room temperature has crystalline and amorphous region, along

with the amorphous region is capable of conducting Li^+ by intrachain and interchain hopping as shown in figure 6. However, under room temperature, its conductivity is at the range of 10^{-8} to 10^{-6} S/cm, which is not even close to sufficient for effective Li^+ transport. Adding soluble Li salts into PEO increases the amorphous region for Li^+ conduction. As stated at the solvation of salt in polymer section, TFSI has the largest dissociation constant compared to the common Li salts in polymer, the question now is add how much of the salt will provide highest conductivity. Figure 7 shows the phase diagram for PEO/LiTFSI system. From the phase diagram of PEO/LiTFSI binary system, a 6 to 10 EO to Li ratio belongs to a so-called “crystallinity gap”^[26], which is formed by retarded growth of crystalline phase where the amorphous state favors remaining at its amorphous state. Based on the above criteria, we choose a 10 EO to Li ratio, which correspond to a 6 wt% PEO to 4 wt% LiTFSI to form a $\text{PEO}_{10}\text{LiTFSI}$ matrix for the gel electrode fabrication.

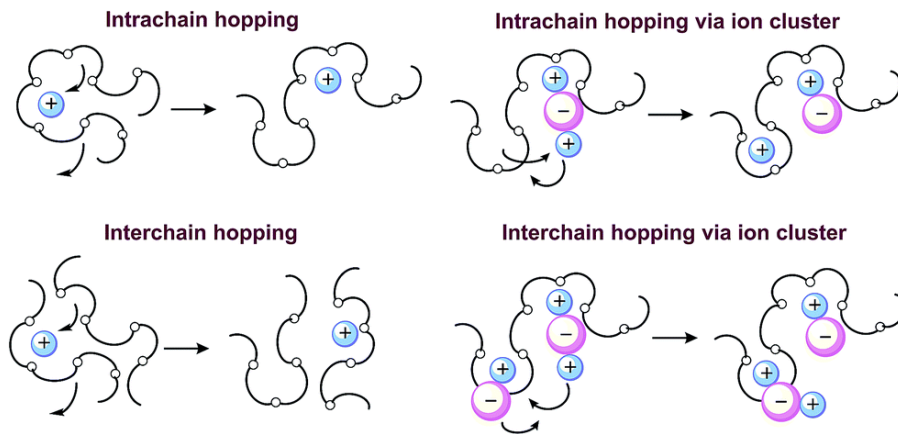


Figure 6. PEO Li^+ conducting mechanism^[24]

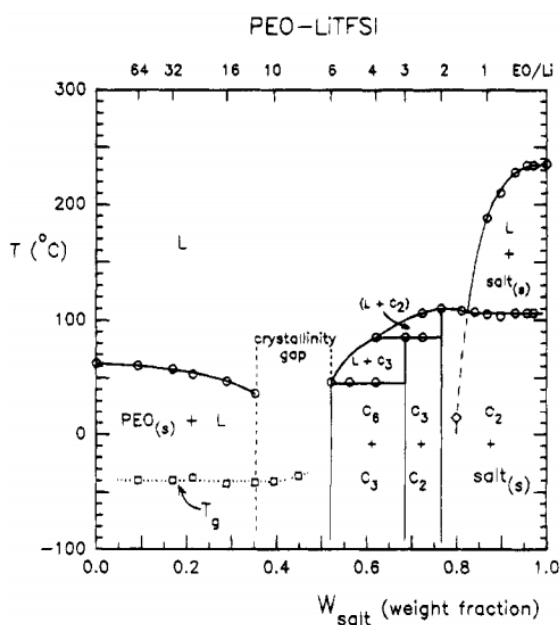


Figure 7. PEO/LiTFSI phase diagram^[26]

2.2 Gel Polymer Electrolyte

PEO is a good candidate of gel polymer electrolyte due to its capability of swelling. Gel polymer electrolyte utilizes a polymer within which confines a certain amount of electrolyte, and serves as both the separator and electrolyte in a cell. Gel polymer electrolyte only requires scarce amount of electrolyte and still has comparable conductivity. It is safer than liquid electrolyte and has higher conductivity than solid electrolyte. The increased safety comes from fewer amounts of flammable electrolyte and the ability to confine the electrolyte within the gel which acts as a barrier for the electrolyte to evaporate. In the case of battery failure such as short circuit, the evaporated electrolyte is easy to catch on fire. Figure 8 shows a systematic thermogravimetric curve comparison between a gel polymer electrolyte and a separator soaked in the same amount of liquid electrolyte^[27]. Under elevated temperature, the liquid electrolyte in the separator is quick to evaporate, causing fire hazard. Gel polymer electrolyte requires much higher temperature to lose the inside liquid electrolyte. Figure 9 illustrates a combustion test of a PVDF-

SiO₂ gel polymer electrolyte, and a separator soaked in the same amount of liquid electrolyte^[28]. The separator caught on fire in less than 3 seconds, while the gel polymer electrolyte not only did it not catch on fire but also not shrink, which reduces the possibility of battery short circuit that would further lead to a thermal runaway. There are generally two types of gel polymer electrolyte^[29]:

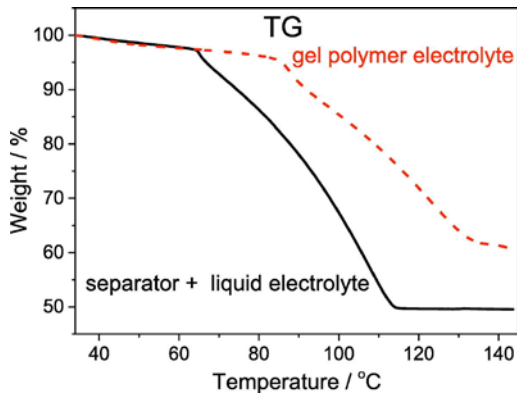


Figure 8. Schematic of thermogravimetric curve of gel polymer electrolyte^[27]

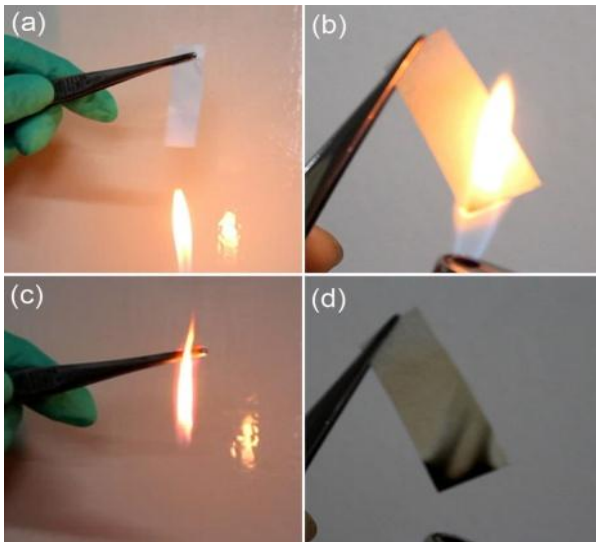


Figure 9. Combustion test Celgard 2730 and PVDF-GFM gel polymer electrolyte^[28]

Physical gels—simply soak the polymer with the electrolyte to form the gel. A typical procedure is solution casting which dissolve the polymer in an appropriate solvent and cast the polymer on a PTFE plate and then add the electrolyte onto the film and leave it for a few hours to

let the polymer intake the electrolyte and form a gel. The advantage of physical gels is the simplicity in preparation, while its drawback is that because of the swelling of the polymer, its mechanical strength decays. Adding inorganic fillers such as SiO_2 , Al_2O_3 is found to be improving the mechanical strength^[30, 31]. Another way of improving the mechanical strength of the gel polymer electrolyte is to crosslink the polymer with an appropriate initiator and crosslinker to form a chemical gel^[32].

Polyethylene oxide (PEO) as a Li^+ conductive polymer has demonstrated its use in gel polymer electrolyte and solid state electrolyte. It has been commercialized as the gel polymer electrolyte in LiFePO_4 batteries with cycling voltage of 2.8-3.6 V. However, its compatibility with layered oxide material such as LiCoO_2 is still an open question^{[33] [34, 35]}. Shiro Seki et al^[35] used PEO as the electrolyte for LiCoO_2 battery and the battery delivered no capacity after 12th cycle. Therefore the author concluded that PEO is not stable to 4 V vs. Li/Li^+ . To the best of our knowledge, there is lack of demonstrating of PEO compatibility with layered oxide material due to the concern of its stability with higher voltage.

2.4 Experimental Procedure of PEO Compatibility Study with NMC Cycling Under 3-4.3 V

In order to verify the compatibility of PEO with NMC 111, following concept of gel polymer electrolyte and keeping the sake of preparation simplicity, we utilized PEO as both the binder and the liquid electrolyte reservoir for a NMC half cell. This process combines the cathode slurry making and gel polymer electrolyte making into one step---gel polymer electrode making.

2.4.1 Gel Polymer Electrode Fabrication

LiTFSI (Bis(trifluoromethane)sulfonimide lithium salt, Sigma Aldrich) salt was dried inside of a glove box under 120 °C overnight. PEO (Average MW 2,000,000, Aldrich Chemistry) was dried under 55 °C in a vacuum oven overnight then transferred into the glove box for prevention of water absorption. 6 wt% PEO and 4wt% LiTFSI were dissolved in Acetonitrile (ACN, 99.8% purity, Sigma Aldrich) to form a polymer matrix with salt as plasticizer---PEO₁₀LiTFSI. Then mixed with 80% LiNi_{1/3}Mn_{1/3}Co_{1/3}O₂ (NMC111,Toda) and 7% Ketchen black (Alfa Aesar) and 3% MWCNT(Alfa Aesar) using a stir bar for 3hrs forming a uniform slurry. Then cast the slurry onto an Al current collector using a Dr. blade. The slurry was dried under 55 °C in the vacuum oven overnight.

2.4.2 Battery Assembly

The cathode is assembled in a 2032 battery using Li metal as the counter electrode. The electrolyte was LP 40 (1M LiPF₆ in EC/DEC 1:1 v/v).The amount of electrolyte added in the gel polymer electrode is with a ratio of 4:1 with regard to active material. To speed up the electrolyte intake of PEO, LP 40 was added on the cathode side. Before charge and discharge cycling, the cells were rested for 4.5 hours. The cycling was performed using LAND (Model:CT2001A/CT2001C, Wuhan LAND electronics).

2.5 Results and Discussion

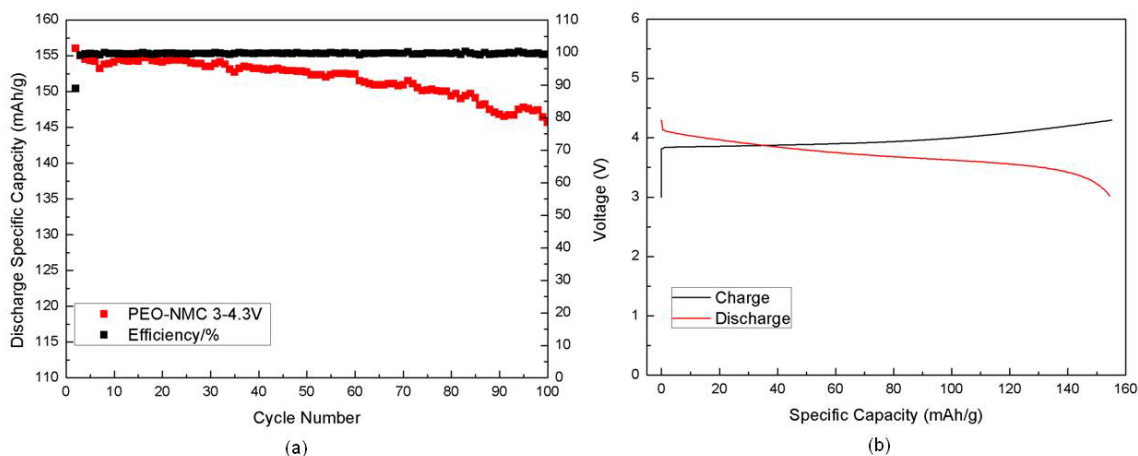


Figure 10. (a) Cycling performance of PEO-NMC cell, 2.608 mg mass loading, 10 μ L of LP 40 added, cycling under 3-4.3V for 100 cycles, 0.1C first cycle and 1C the rest of the cycles (b) 4th cycle charge-discharge curve of the cell in figure 12 (a)

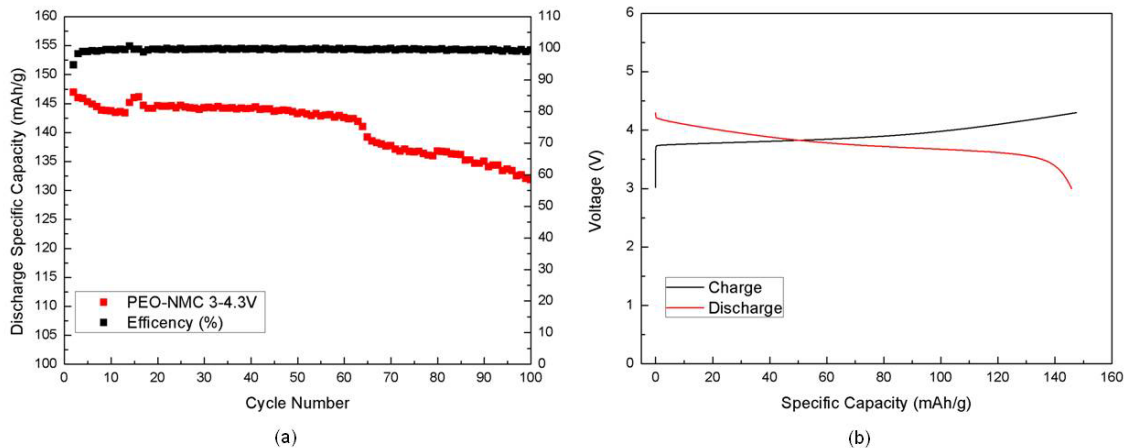


Figure 11. (a) Cycling performance of PEO-NMC cell, 7.361 mg mass loading, 28 μ L of LP 40 added, cycling under 3-4.3V for 100 cycles, 0.1C first cycle and 0.2C the rest of the cycles (b) 4th cycle charge-discharge curve of the cell in figure 13 (a)

The first cycle capacity of PEO-NMC was 156 mAh/g as shown in figure 12 (a), assuming it takes 3 cycles to activate the cell, the 4th cycle charge-discharge curve is shown in figure 12 (b). Compared to published data of a NMC111 cathode with PVDF binder under the same C rate and comparable voltage range by Ohzuku T and Makimura Y ^[8], the cell using PEO as a binder has

comparable capacity. For the PEO-NMC cell, 50th cycle capacity retention was 97.88%, by 100th cycle capacity retention was 93.39%.

Making thicker cathode has been a challenge for NMC cathode research due to cracking issue and electrolyte wettability difficulties. However, making thicker cathode is necessary for future full cell fabrication, which cathode is the limitation to the overall capacity. Graphite for example, has a theoretical capacity of 372 mAh/g while NMC only has less than half of the capacity compared to graphite, therefore the loading of NMC has to be more than twice than that of graphite in order to deliver comparable capacity in a future full cell. Figure 13 shows a PEO-NMC cell cycling performance with twice the amount of loading than that of figure 12. The cathode loading was 7.361mg, which correspond to 6.51 mg/cm², electrolyte to active mass ratio was 4:1. The first cycle capacity was 155 mAh/g and then after increasing the C rate from 0.1C to 1C, the capacity decreased to 147 mAh/g on the second cycle. Thicker electrodes require more time for charge transfer and diffusion, increasing the C rate by 10 times of the second cycle may increase the difficulty for charge transfer. The 50th cycle and 100th cycle capacity retention was 92.25% and 85%, respectively.

Table 3. Examples of different active mass and electrolyte amount for PEO-NMC and corresponding capacity

Mass Loading (mg)	Binder Amount (mg)	Electrolyte Amount Added (uL)	Electrolyte to Mass Ratio (uL/mg)	1st Cycle Capacity (mAh/g)	4th Cycle Capacity (mAh/g)
2.608	0.196	10	4	156	154
3.568	0.357	14	4	163	133
7.361	0.552	29	4	155	146
10.591	0.794	20	2	153	43
10.74	0.022	20	2	70	58

Table 3 lists the different active mass and electrolyte amount for PEO-NMC and corresponding capacity. For the case of above 10 mg of mass loading, 20 uL of electrolyte seems

to be insufficient while for mass loading of 2-3 mg, a electrolyte to mass ratio of 4:1 seems to be sufficient. The upper and lower limitation of electrolyte amount and mass loading is needed for future work. Though we might not have a conclusion how much electrolyte and mass loading is the limit, PEO₁₀LiTFSI is compatible with NMC 111 with the ability to cycle under 3-4.3 V.

Chapter 3 PEO Stability with Electrolyte under Battery Cycling

We have now illustrated the compatibility of PEO with layered oxide material NMC. Using PEO as the binder and also the liquid electrolyte reservoir, a far less amount of liquid electrolyte is needed for the battery to have comparable capacity with a normal NMC cell using a PVDF binder. The next step is to isolate PEO and study its stability during normal charge-discharge process with sufficient amount of electrolyte. For sake of comparison, PVDF is chosen as the control sample

3.1 Experimental

3.1.1 Polymer Film Fabrication

To study the stability of PEO under 3-4.5 V with LP 40 electrolyte, the polymer (PEO, Average MW 2,000,000, Aldrich Chemistry) was drop casted onto a 12 mm Al current collector. The mass of each film was controlled under 0.5 mg/cm^2 . PVDF-HFP (Kynar Flex 2801) was selected as a control sample. The solvent for PEO was deionized water, for PVDF was NMP. During battery assembly, each electrode was added 30 μL of LP 40 1M LiPF_6 in EC/DEC 1:1 v/v) electrolyte.

3.1.2 Cyclic Voltammetry

Each polymer film was then assembled into a 2032 cell with Li metal as a counter electrode. The CV testing was performed using Arbin. The scan rates were 5 mV, 2 mV, 1mV and 0.5 mV for 10 cycles from 3V to 4.5V.

3.1.3 X-ray Photoelectron Spectroscopy (XPS) Measurement Sample Preparation

The cycled batteries were held at 4.3 V for 10 hours using an electrochemical workstation before disassembly to place the batteries under the same state of charge. Then the batteries were disassembled by a 2032 battery dissembler in a glove box. The polymer film with the Al current collector was taken out of the 2032 battery by dissembling the battery with a dissembler. All the

electrodes were immersed in DMC solvent for 20 min to remove remaining LiPF_6 salt, and then the electrodes were dried under room temperature in the glove box overnight. Then the electrodes were placed into an air-tight argon flow bag for XPS analysis.

3.2 Result and Discussion

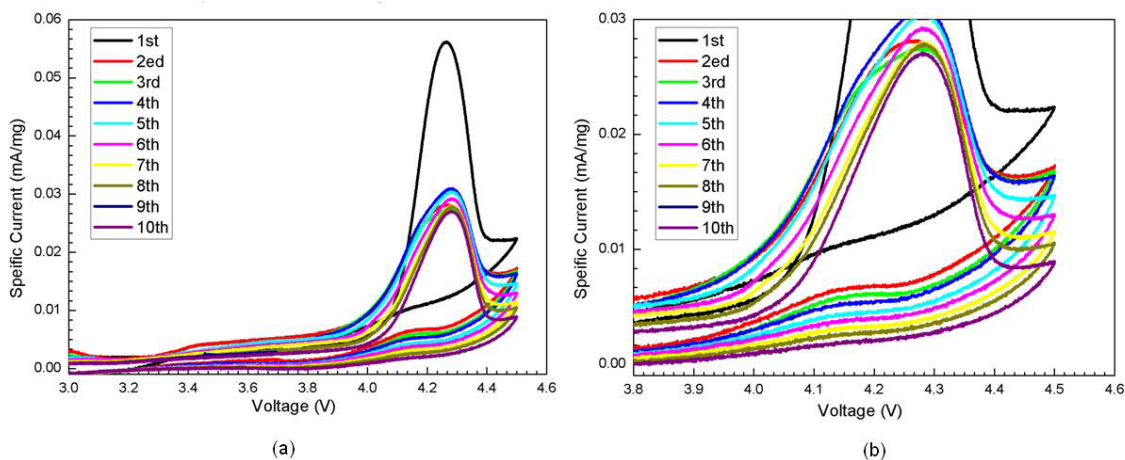


Figure 12. (a) Cyclic voltammogram of PVDF with 30 uL LP 40 under scan rate of 0.5 mV (b) Zoomed in on figure 14 (a)

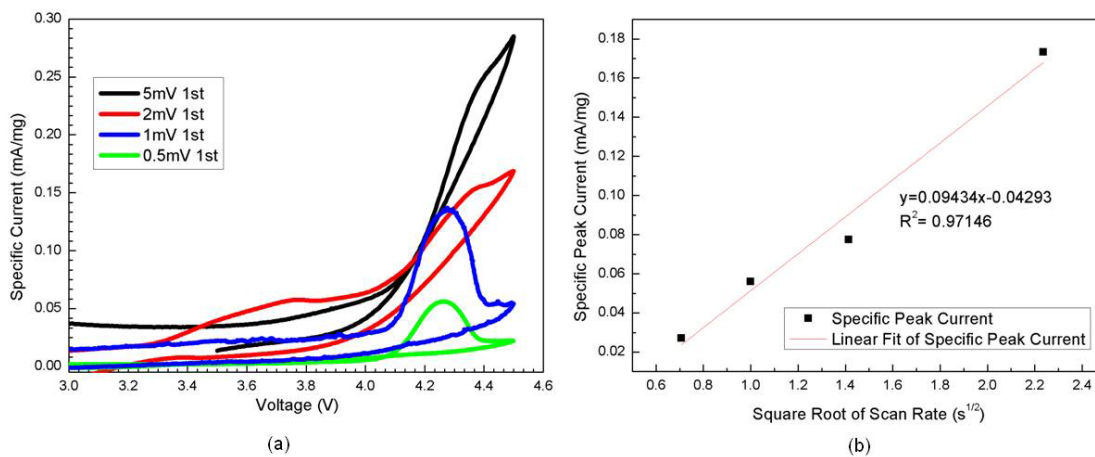


Figure 13. (a) Cyclic voltammogram of PVDF with 30 uL electrolyte under scan rate of 5 mV/s, 2 mV/s, 1 mV/s and 0.5 mV/s (b) Plot of specific peak current of different scan rates vs. square root of scan rate

Figure 12 shows the cyclic voltammogram of PVDF with 30 uL of LP 40 under scan rate of

0.5 mV, as we could see from figure 14 (b), there is a trend of peak current decreasing with increase of scan rate, expect for a sudden current jump for the 9th cycle. There might be a passivation layer formed on the surface of PVDF with the electrolyte. Figure 13 plots the peak current of different scan rates of 5 mV/s, 2 mV/s, 1 mV/s and 0.5 mV/s. Plotting the peak current vs. the square root of scan rate, according to $i_p = a v^b$, which a is a constant and b is usually from 0 to 1^[36], the best fitting of this data shows that b value is close to 0.5, which mean this process is diffusion controlled which is in agreement with possible forming of a passivation layer.

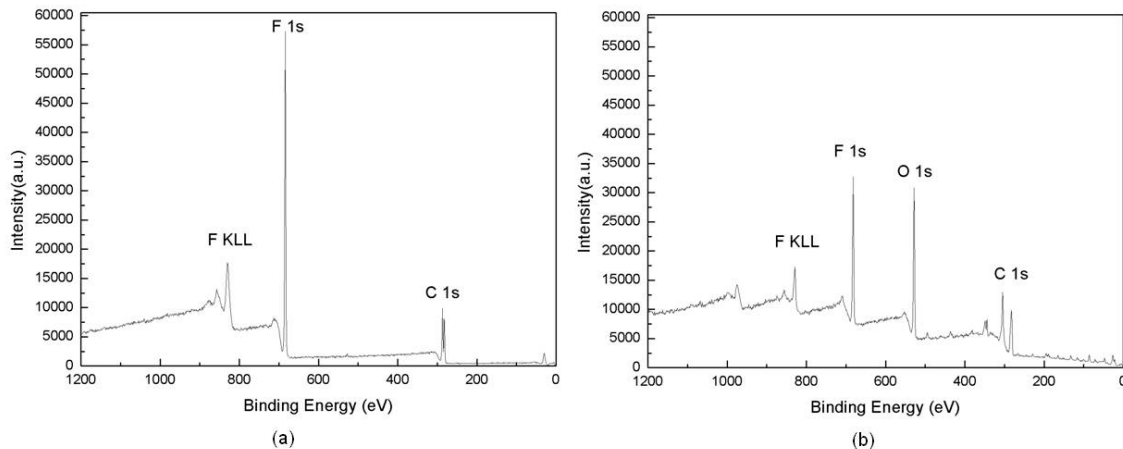


Figure 14. (a) Pristine PVDF XPS spectra (b) PVDF after cycling XPS spectra

Figure 14 shows a comparison of XPS spectra of a pristine PVDF film coated on Al current collector and a PVDF cycled with 30 μ L of LP 40 for 10 cycles under 3-4.3 V, with 1 mV/s scan rate and held at 4.3V for 10 hours. We can see that after cycling, there is presence of O element on the PVDF film.

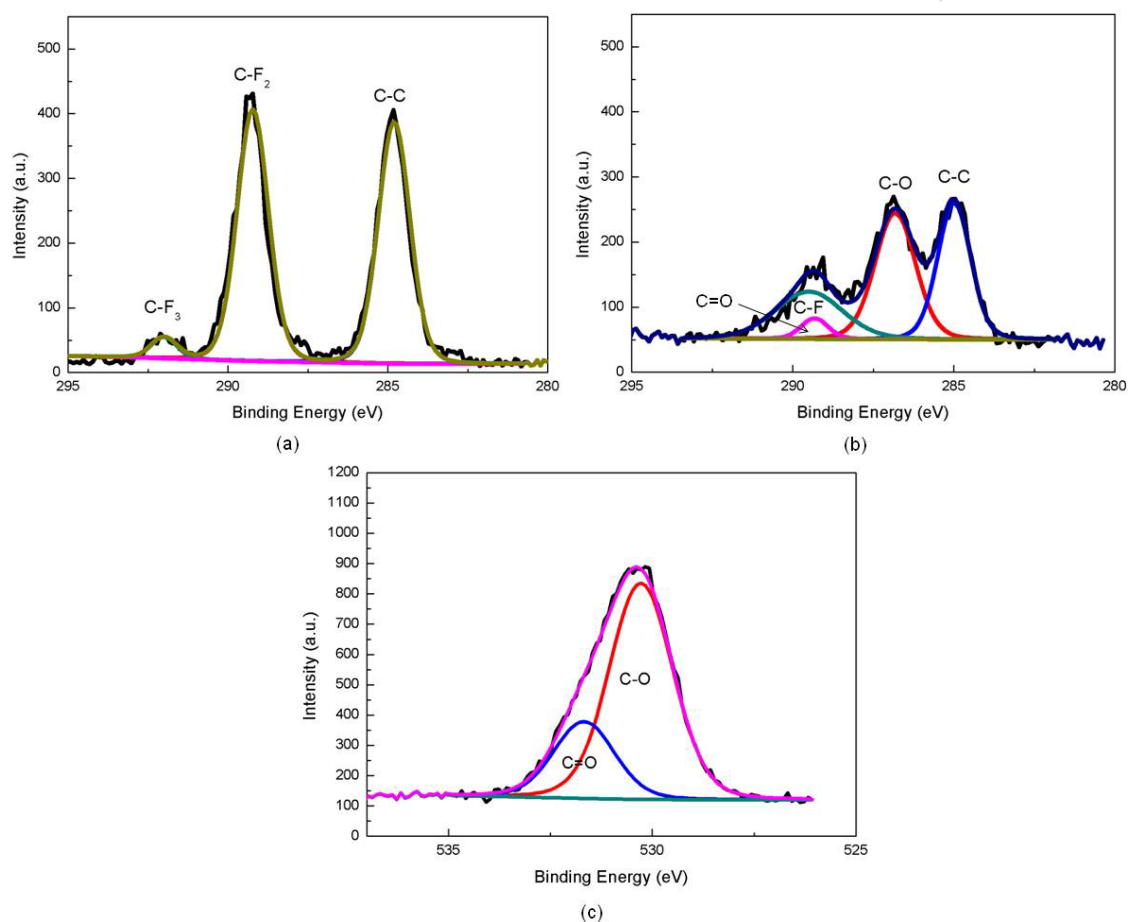


Figure 15. (a) Pristine PVDF C 1s XPS spectra (b) PVDF after cycled with 30 uL LP 40 C 1s XPS spectra (c) PVDF after cycled with 30 uL LP 40 O 1s XPS spectra

Figure 15 shows the C 1s peak of the two PVDF samples in figure 16, which the peaks are identified based on the XPS data base^[37, 38], and calibrated XPS spectra based on C-C (284.8 eV), after cycling, there were peaks of C=O (~288.5 eV) and C-O (~286 eV) for PVDF sample. It is in agreement with the O 1s spectra as shown in figure 17 (c), there are two peaks that contribute to this peak signal: the O 1s C=O (~533 eV) and C-O (531.5 eV). Since there is no oxygen element in PVDF itself, the oxygen peaks come from liquid electrolyte decomposition or possible interaction with PVDF.

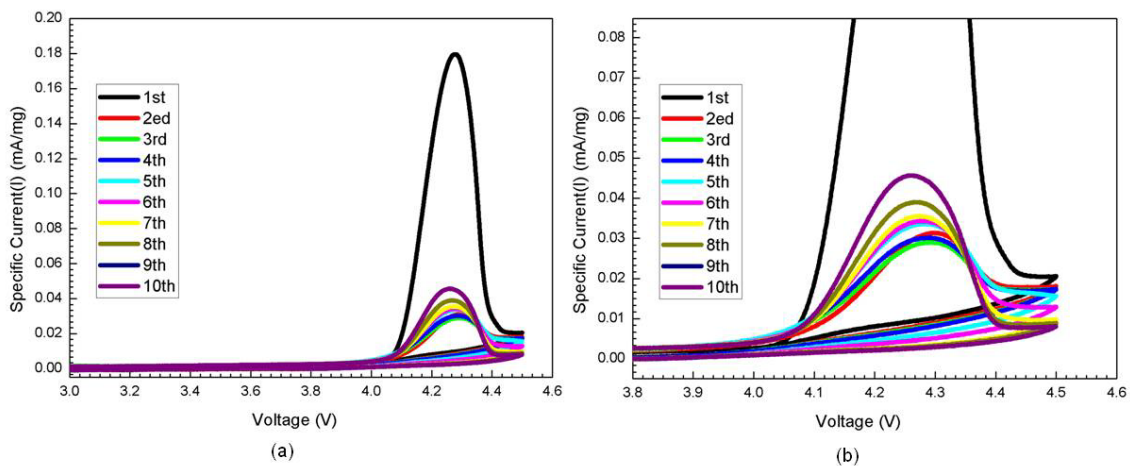


Figure 16. (a) Cyclic voltammogram of PEO with 30 uL LP 40 under scan rate of 0.5 mV (b) Zoomed in on figure 18 (a)

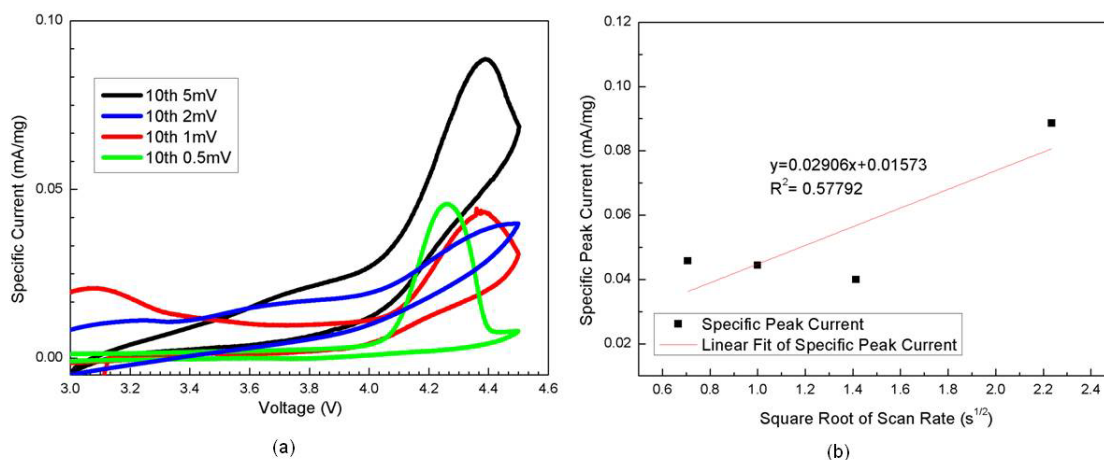


Figure 17. (a) Cyclic voltammogram of PEO with 30 uL electrolyte under scan rate of 5 mV/s, 2 mV/s, 1 mV/s and 0.5 mV/s (b) Plot of specific peak current of different scan rates vs. square root of scan rate

Figure 16 shows the cyclic voltammogram of PEO with 30 uL of LP 40 under scan rate of 0.5 mV, contrary to figure 14 (b), there no obvious trend of peak current decreasing with increase of scan rate, the relationship between peak current with respect to the cycle number seems to be random. Figure 17 plots the peak current of the PEO system with different scan rates of 5 mV/s, 2 mV/s, 1 mV/s and 0.5 mV/s. Plotting the peak current vs. the square root of scan rate,

the data does not seem to fit the relationship of $i_p = a v^b$, which a is a constant and b is usually from 0 to 1^[36]. It is possible that the constant segmental motion of PEO prevents the formation of a passivation layer on the surface.

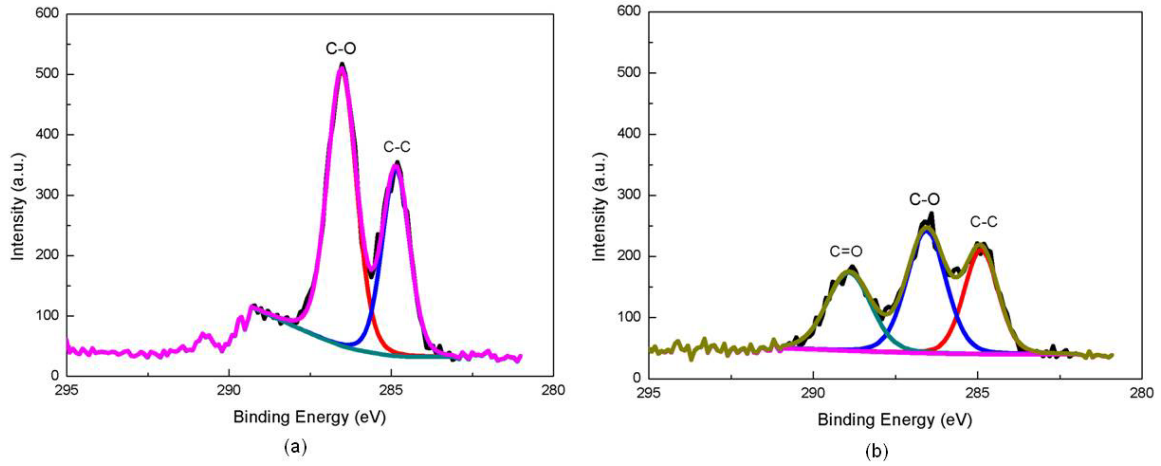


Figure 18. (a) Pristine PEO C 1s XPS spectra (b) PEO after cycled with 30 uL LP 40 C 1s XPS spectra

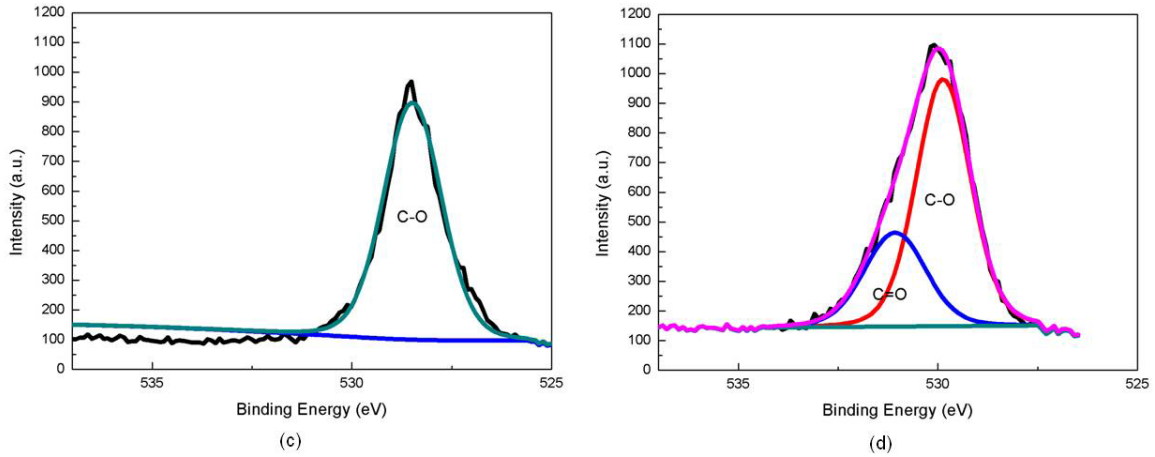


Figure 19. (a) Pristine PEO O 1s XPS spectra (b) PEO after cycled with 30 uL LP 40 O 1s XPS spectra

Figure 18 shows the C 1s peak of the pristine PEO film on Al current collector and the C 1s peak of PEO film after the cycling. Based on the XPS data base^[37, 38], and calibrated XPS spectra based on C-C (284.8 eV), after cycling, C=O (~288.5 eV) was detected for PEO sample. It is in

agreement with the PEO O 1s spectra as shown in figure 19 (c), there are two peaks that contribute to this peak signal: the O 1s C=O (~533 eV) and C-O (531.5 eV). The O 1s peak of PEO after cycling is similar to that of PVDF, which means similar composition of liquid electrolyte decomposition product was formed on the surface of the binders.

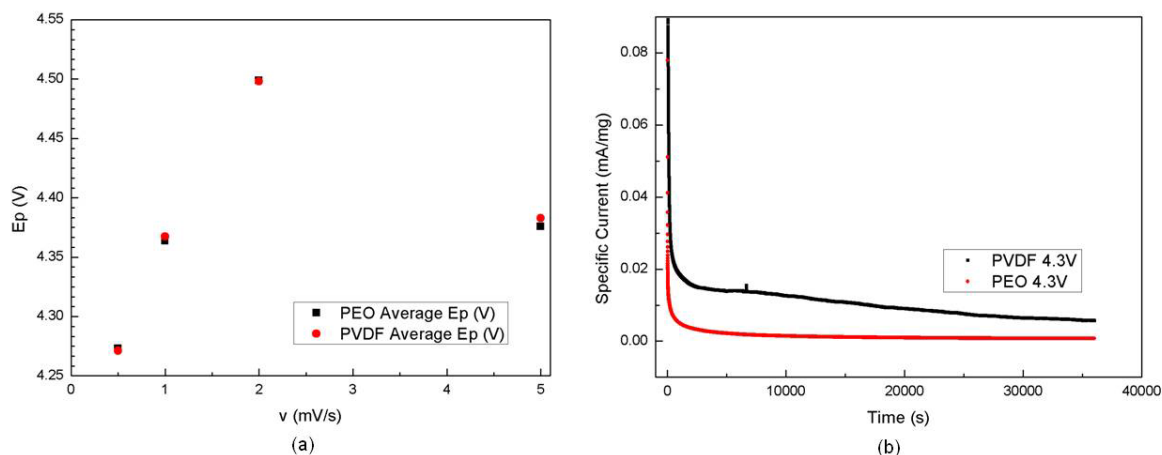


Figure 20. (a) PEO and PVDF with 30 μ L LP 40, 10 cycles of CV scan average peak current vs. scan rate (b) PVDF and PEO with 30 μ L LP 40 after 10 cycles of CV scan held at 4.3 V for 10 hours chronoamperogram

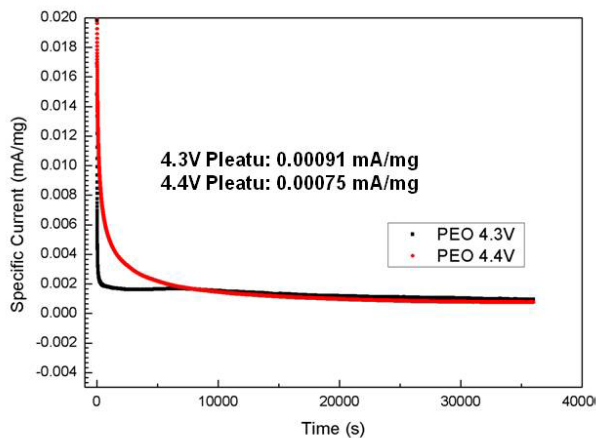


Figure 21. PEO 4.3 and 4.4V chronoamperogram

Figure 20(a) compares the average peak voltage of each polymer and plot against scan rate.

Both of the binder shows the same trend, which further supports the hypothesis that the current signal from the cyclic voltammograms are possibly from the liquid electrolyte itself. Figure 20 (b) compares the chronoamperogram signal where both of the binders were held under 4.3 V for 10 hours. PVDF did not seem to reach an absolute plateau during the first 5 hours, while PEO reached a plateau in a fairly short time compared to PVDF. From figure 20 (b), PEO might be more stable than PVDF in 30 μ L of LP 40 under 4.3 V. Figure 22 shows the chronoamperogram of a cycled PEO cell under 1 mV for 10 cycles which was then held under 4.3 V and 4.4 V for 10 hours. From the chronoamperogram, the cell reached plateau under fairly short amount of time which indicates that the system of PEO film with LP 40 electrolyte is stable up to 4.4 V.

Conclusion

Our study shows that PEO as a binder and liquid electrolyte reservoir is capable of reducing the liquid electrolyte usage in a Li-ion battery cathode, which contributes to building a safer battery. Despite the concerns of PEO stability with layered oxide material under voltage above 4 V, the PEO-NMC 111 cell illustrates reasonable charge-discharge capacity and cycling efficiency under 3 to 4.3 V for 100 cycles. We then isolated the polymer PEO and studied its electrochemical stability under cycling of 3 to 4.5 V. From the chronoamperogram, PEO with LP 40 electrolyte system is stable at least up to 4.4 V. It is likely that there are interactions or interfaces formed between PEO/LP 40 or PEO/NMC/LP 40, which the interface compositions are stable under the cycling voltage. Based on our findings, although further characterizations of the PEO/NMC/LP 40 is desired, it is safe to conclude that PEO has acceptable stability as an ionic conducting binder for Li-ion battery cathode.

References

- [1] R.T. Doucette, M.D. McCulloch, Modeling the CO₂ emissions from battery electric vehicles given the power generation mixes of different countries, *Energy Policy*, 39 (2011) 803-811.
- [2] J.M. Tarascon, M. Armand, Issues and challenges facing rechargeable lithium batteries, *Nature*, 414 (2001) 359-367.
- [3] R.E. Stoll, F. von Linde, Hydrogen - what are the costs?, *Hydrocarb Process*, 79 (2000) 42-+.
- [4] W. Qi, J.G. Shapter, Q. Wu, T. Yin, G. Gao, D.X. Cui, Nanostructured anode materials for lithium-ion batteries: principle, recent progress and future perspectives, *Journal of Materials Chemistry A*, 5 (2017) 19521-19540.
- [5] B. Xu, D.N. Qian, Z.Y. Wang, Y.S.L. Meng, Recent progress in cathode materials research for advanced lithium ion batteries, *Mat Sci Eng R*, 73 (2012) 51-65.
- [6] A. Van der Ven, M.K. Aydinol, G. Ceder, G. Kresse, J. Hafner, First-principles investigation of phase stability in Li_xCoO₂, *Phys Rev B*, 58 (1998) 2975-2987.
- [7] N. Nitta, F.X. Wu, J.T. Lee, G. Yushin, Li-ion battery materials: present and future, *Materials Today*, 18 (2015) 252-264.
- [8] T. Ohzuku, Y. Makimura, Layered lithium insertion material of LiCo_{1/3}Ni_{1/3}Mn_{1/3}O₂ for lithium-ion batteries, *Chem Lett*, DOI (2001) 642-643.
- [9] Z.L. Liu, A.S. Yu, J.Y. Lee, Synthesis and characterization of LiNi_{1-x-y}CoxMnyO₂ as the cathode materials of secondary lithium batteries, *Journal of Power Sources*, 81 (1999) 416-419.
- [10] K. Xu, Nonaqueous liquid electrolytes for lithium-based rechargeable batteries, *Chemical Reviews*, 104 (2004) 4303-4417.
- [11] K. Xu, Electrolytes and Interphases in Li-Ion Batteries and Beyond, *Chemical Reviews*, 114 (2014) 11503-11618.
- [12] V. Etacheri, R. Marom, R. Elazari, G. Salitra, D. Aurbach, Challenges in the development of advanced Li-ion batteries: a review, *Energy & Environmental Science*, 4 (2011) 3243-3262.

- [13] S.L. Chou, Y. Pan, J.Z. Wang, H.K. Liu, S.X. Dou, Small things make a big difference: binder effects on the performance of Li and Na batteries, *Physical chemistry chemical physics : PCCP*, 16 (2014) 20347-20359.
- [14] G. Liu, H. Zheng, X. Song, V.S. Battaglia, Particles and Polymer Binder Interaction: A Controlling Factor in Lithium-Ion Electrode Performance, *Journal of the Electrochemical Society*, 159 (2012) A214-A221.
- [15] Y. Shi, X. Zhou, G. Yu, Material and Structural Design of Novel Binder Systems for High-Energy, High-Power Lithium-Ion Batteries, *Acc Chem Res*, 50 (2017) 2642-2652.
- [16] K. Ozawa, Lithium-Ion Rechargeable Batteries with LiCoO_2 and Carbon Electrodes - the LiCoO_2 C System, *Solid State Ionics*, 69 (1994) 212-221.
- [17] K. Wu, J. Yang, Y. Zhang, C.Y. Wang, D.Y. Wang, Investigation on $\text{Li}_4\text{Ti}_5\text{O}_{12}$ batteries developed for hybrid electric vehicle, *J Appl Electrochem*, 42 (2012) 989-995.
- [18] K.C. Kil, U. Paik, Lithium salt of carboxymethyl cellulose as an aqueous binder for thick graphite electrode in lithium ion batteries, *Macromol Res*, 23 (2015) 719-725.
- [19] Y. Sun, L. Zhao, H.L. Pan, X. Lu, L. Gu, Y.S. Hu, H. Li, M. Armand, Y. Ikuhara, L.Q. Chen, X.J. Huang, Direct atomic-scale confirmation of three-phase storage mechanism in $\text{Li}_4\text{Ti}_5\text{O}_{12}$ anodes for room-temperature sodium-ion batteries, *Nature Communications*, 4 (2013).
- [20] J. Li, R.B. Lewis, J.R. Dahn, Sodium carboxymethyl cellulose - A potential binder for Si negative electrodes for Li-ion batteries, *Electrochem Solid St*, 10 (2007) A17-A20.
- [21] A. Magasinski, B. Zdyrko, I. Kovalenko, B. Hertzberg, R. Burtovyy, C.F. Huebner, T.F. Fuller, I. Luzinov, G. Yushin, Toward Efficient Binders for Li-Ion Battery Si-Based Anodes: Polyacrylic Acid, *ACS applied materials & interfaces*, 2 (2010) 3004-3010.
- [22] J. Hassoun, D.J. Lee, Y.K. Sun, B. Scrosati, A lithium ion battery using nanostructured Sn-C anode, LiFePO_4 cathode and polyethylene oxide-based electrolyte, *Solid State Ionics*, 202 (2011) 36-39.
- [23] J.Z. Chen, W.A. Henderson, H.L. Pan, B.R. Perdue, R.G. Cao, J.Z. Hu, C. Wan, K.S. Han, K.T. Mueller, J.G. Zhang, Y.Y. Shao, J. Liu, Improving Lithium-Sulfur Battery Performance under Lean Electrolyte through Nanoscale Confinement in Soft Swellable Gels, *Nano Letters*, 17 (2017) 3061-3067.

- [24] Z.G. Xue, D. He, X.L. Xie, Poly(ethylene oxide)-based electrolytes for lithium-ion batteries, *Journal of Materials Chemistry A*, 3 (2015) 19218-19253.
- [25] S. Sylla, J.Y. Sanchez, M. Armand, Electrochemical Study of Linear and Cross-Linked PEO-Based Polymer Electrolytes, *Electrochimica Acta*, 37 (1992) 1699-1701.
- [26] S. Lascaud, M. Perrier, A. Vallee, S. Besner, J. Prudhomme, M. Armand, Phase-Diagrams and Conductivity Behavior of Poly(Ethylene Oxide) Molten-Salt Rubbery Electrolytes, *Macromolecules*, 27 (1994) 7469-7477.
- [27] S.S. Liang, W.Q. Yan, X. Wu, Y. Zhang, Y.S. Zhu, H.W. Wang, Y.P. Wu, Gel polymer electrolytes for lithium ion batteries: Fabrication, characterization and performance, *Solid State Ionics*, 318 (2018) 2-18.
- [28] Y.S. Zhu, F.X. Wang, L.L. Liu, S.Y. Xiao, Y.Q. Yang, Y.P. Wu, Cheap glass fiber mats as a matrix of gel polymer electrolytes for lithium ion batteries, *Sci Rep-Uk*, 3 (2013).
- [29] A. Arya, A.L. Sharma, Polymer electrolytes for lithium ion batteries: a critical study, *Ionics*, 23 (2017) 497-540.
- [30] S.K. Fullerton-Shirey, J.K. Maranas, Structure and Mobility of PEO/LiClO₄ Solid Polymer Electrolytes Filled with Al₂O₃ Nanoparticles, *J Phys Chem C*, 114 (2010) 9196-9206.
- [31] Z.W. Bai, B.E. Taylor, J.M. Haag, T.D. Dang, M.F. Durstock, In-situ generated PEO-SiO₂ nanocomposite electrolytes for lightweight, flexible batteries, *Abstr Pap Am Chem S*, 241 (2011).
- [32] R. Uchiyama, K. Kusagawa, K. Hanai, N. Imanishi, A. Hirano, Y. Takeda, Development of dry polymer electrolyte based on polyethylene oxide with co-bridging agent crosslinked by electron beam, *Solid State Ionics*, 180 (2009) 205-211.
- [33] D.T. Hallinan, A. Rausch, B. McGill, An electrochemical approach to measuring oxidative stability of solid polymer electrolytes for lithium batteries, *Chem Eng Sci*, 154 (2016) 34-41.
- [34] J. Ma, Z.L. Liu, B.B. Chen, L.L. Wang, L.P. Yue, H.S. Liu, J.J. Zhang, Z.H. Liu, G.L. Cui, A Strategy to Make High Voltage LiCoO₂ Compatible with Polyethylene Oxide Electrolyte in All-Solid-State Lithium Ion Batteries, *Journal of the Electrochemical Society*, 164 (2017) A3454-A3461.

- [35] S. Seki, Y. Kobayashi, H. Miyashiro, Y. Mita, T. Iwahori, Fabrication of high-voltage, high-capacity all-solid-state lithium polymer secondary batteries by application of the polymer electrolyte/inorganic electrolyte composite concept, *Chem Mater*, 17 (2005) 2041-2045.
- [36] N. Elgrishi, K.J. Rountree, B.D. McCarthy, E.S. Rountree, T.T. Eisenhart, J.L. Dempsey, A Practical Beginner's Guide to Cyclic Voltammetry, *Journal of Chemical Education*, 95 (2017) 197-206.
- [37] H. Nohira, W. Tsai, W. Besling, E. Young, J. Petry, T. Conard, W. Vandervorst, S. De Gendt, M. Heyns, J. Maes, M. Tuominen, Characterization of ALCVD-Al₂O₃ and ZrO₂ layer using X-ray photoelectron spectroscopy, *J Non-Cryst Solids*, 303 (2002) 83-87.
- [38] A.V. Shchukarev, D.V. Korolkov, XPS study of group IA carbonates, *Cent Eur J Chem*, 2 (2004) 347-362.
- [39] I. Kovalenko, B. Zdyrko, A. Magasinski, B. Hertzberg, Z. Milicev, R. Burtovyy, I. Luzinov, G. Yushin, A Major Constituent of Brown Algae for Use in High-Capacity Li-Ion Batteries, *Science*, 334 (2011) 75-79.
- [40] S.S. Zhang, T.R. Jow, Study of poly (acrylonitrile-methyl methacrylate) as binder for graphite anode and LiMn₂O₄ cathode of Li-ion batteries, *Journal of Power Sources*, 109 (2002) 422-426.
- [41] A. Chandra, PEO-PVP blended Na⁺ ion conducting solid polymeric membranes, *Chinese J Polym Sci*, 31 (2013) 1538-1545.
- [42] L. Chen, Y.T. Li, S.P. Li, L.Z. Fan, C.W. Nan, J.B. Goodenough, PEO/garnet composite electrolytes for solid-state lithium batteries: From "ceramic-in-polymer" to "polymer-in-ceramic", *Nano Energy*, 46 (2018) 176-184.
- [43] S.J. Chen, J.Y. Wang, Z.H. Zhang, L.B. Wu, L.L. Yao, Z.Y. Wei, Y.H. Deng, D.J. Xie, X.Y. Yao, X.X. Xu, In-situ preparation of poly(ethylene oxide)/Li₃PS₄ hybrid polymer electrolyte with good nanofiller distribution for rechargeable solid-state lithium batteries, *Journal of Power Sources*, 387 (2018) 72-80.
- [44] Z.Y. Cui, Y.Y. Xu, L.P. Zhu, J.Y. Wang, Z.Y. Xi, B.K. Zhu, Preparation of PVDF/PEO-PPO-PEO blend microporous membranes for lithium ion batteries via thermally induced phase separation process, *J Membrane Sci*, 325 (2008) 957-963.

- [45] M.A.K.L. Dissanayake, Nano-composite solid polymer electrolytes, *Solid State Ionics: Trends in the New Millennium, Proceedings*, DOI (2002) 251-262.
- [46] S. Gomari, M. Esfandeh, I. Ghasemi, All-solid-state flexible nanocomposite polymer electrolytes based on poly(ethylene oxide): Lithium perchlorate using functionalized graphene, *Solid State Ionics*, 303 (2017) 37-46.
- [47] Q. Li, N. Imanishi, Y. Takeda, A. Hirano, O. Yamamoto, PEO-based Composite Lithium Polymer Electrolyte, PEO-BaTiO(3)-Li(C(2)F(5)SO(2))(2)N, *Ionics*, 8 (2002) 79-84.
- [48] M. Lu, P.F. Shi, Electrochemical performance of PEO₁₀LiX-Li₂TiO₃ composite polymer electrolytes, *Chinese J Chem*, 22 (2004) 47-50.
- [49] C.Y. Pan, Q. Zhang, Q. Feng, J.H. Gao, Y.M. Zhao, Effect of catalyst on structure of (PEO)₈LiClO₄-SiO₂ composite polymer electrolyte films, *J Cent South Univ T*, 15 (2008) 438-442.
- [50] G.P. Pandey, S.A. Hashmi, R.C. Agrawal, Hot-press synthesized polyethylene oxide based proton conducting nanocomposite polymer electrolyte dispersed with SiO₂ nanoparticles, *Solid State Ionics*, 179 (2008) 543-549.
- [51] P. Ramakrishnan, H. Kwak, Y.H. Cho, J.H. Kim, Ionic Conductivity of Ruddlesden-Popper Layered Perovskites (Li₂SrTa₂O₇, Li₂SrNb₂O₇, and Li₂CaTa₂O₇) with Poly (ethylene oxide) as a Composite Solid Electrolyte, *Chemelectrochem*, 5 (2018) 1265-1271.
- [52] C.V.S. Reddy, G.P. Wu, C.X. Zhao, W. Jin, Q.Y. Zhu, W. Chen, S.I. Mho, Mesoporous silica (MCM-41) effect on (PEO+LiAsF₆) solid polymer electrolyte, *Curr Appl Phys*, 7 (2007) 655-661.
- [53] Z. Ren, K.N. Sun, Y.Y. Liu, X.L. Zhou, N.Q. Zhang, X.D. Zhu, Polymer electrolytes based on poly(vinylidene fluoride-co-hexafluoropropylene) with crosslinked poly(ethylene glycol) for lithium batteries, *Solid State Ionics*, 180 (2009) 693-697.
- [54] H. Zhang, C.Y. Liu, L.P. Zheng, F. Xu, W.F. Feng, H. Li, X.J. Huang, M. Armand, J. Nie, Z.B. Zhou, Lithium bis(fluorosulfonyl)imide/poly(ethylene oxide) polymer electrolyte, *Electrochimica Acta*, 133 (2014) 529-538.
- [55] Y.R. Zhao, Z. Huang, S.J. Chen, B. Chen, J. Yang, Q. Zhang, F. Ding, Y.H. Chen, X.X. Xu, A promising PEO/LAGP. hybrid electrolyte prepared by a simple method for all-solid-state

lithium batteries, *Solid State Ionics*, 295 (2016) 65-71.

[56] Y.R. Zhao, C. Wu, G. Peng, X.T. Chen, X.Y. Yao, Y. Bai, F. Wu, S.J. Chen, X.X. Xu, A new solid polymer electrolyte incorporating $\text{Li}_{10}\text{GeP}_2\text{S}_{12}$ into a polyethylene oxide matrix for all-solid-state lithium batteries, *Journal of Power Sources*, 301 (2016) 47-53.

[57] J. Zheng, M.X. Tang, Y.Y. Hu, Lithium Ion Pathway within $\text{Li}_7\text{La}_3\text{Zr}_2\text{O}_{12}$ -Polyethylene Oxide Composite Electrolytes, *Angew Chem Int Edit*, 55 (2016) 12538-12542.

[58] P. Zhu, C.Y. Yan, M. Dirican, J.D. Zhu, J. Zang, R.K. Selvan, C.C. Chung, H. Jia, Y. Li, Y. Kiyak, N.Q. Wu, X.W. Zhang, $\text{Li}_{0.33}\text{La}_{0.557}\text{TiO}_3$ ceramic nanofiber-enhanced polyethylene oxide-based composite polymer electrolytes for all-solid-state lithium batteries, *Journal of Materials Chemistry A*, 6 (2018) 4279-4285.